Wasit Journal of Engineering Sciences

Journal homepage: https://ejuow.uowasit.edu.iq

Numerical studies on Pulse tube refrigerator and the effect of changing the load of the regenerator on temperatures

Sarah Taher Y Al- lami[1] , and Ali A . F Al- Hamadani[1]

Affiliations

[1] Mechanical Engineering Department, College of Engineering, Wasit University, Wasit, Iraq

Correspondence
Sarah Taher Y Al- lami
sarahtaher301@uowasit.edu.iq

Received
18-September-2023
Revised
15-November-2023
Accepted
28-November-2023

Doi
10.31185/ejuow.Vol11.Iss3.481

Abstract
Devices for cryogenic cooling based on the Stirling cycle include pulse tube refrigerators. They are often employed in a variety of applications, including space exploration, superconductivity, and cryogenic research, where small and dependable cryogenic cooling is necessary. A working gas, commonly helium, is compressed and expanded in cycles within a closed system to operate a pulse tube refrigerator. The goal of theoretical research on pulse tube refrigerators is to comprehend the system's thermodynamic behavior and performance characteristics. In order to obtain greater cooling efficiency and lower temperatures, these studies are strivinge to improve the design parameters and operating conditions. To forecast the system's performance, theoretical models are taking into account a number of variables, including heat transfer, pressure drop, gas dynamics, and fluid characteristics. The outcome demonstrates how a system's temperature gradient. The ansys program was used to conduct a thermal simulation, as well use solidworks to draw geometry design the temperature gradient is 3 W/m^2, reaching 47 K. The heat load increases as the temperature rises, reaching [43,58,79,90,111,156,] K at [3,4,5,6,8,10] W/m^2. With a temperature gradient of 88.034k in the first order and 340 k in the second order, the simulation approach demonstrates that the best scenario achieved 105 K. The best example with a difference in heat load was at 3 W/m^2, reaching 108K, Results revealed a 5% error rate temperature decline at the pulse tube.

Keywords: The pulse tube refrigerator(IPTR) , Inertance tube pulse tube refrigerator (ITPTR), Orifice pulse tube refrigerator (OPTR), the opening heartbeat tube fridge, ANSYS, CFD, Porous media, (CHX)Cold heat exchanger , (AFTC)After cooler , (WHX)Warm heat exchanger.

الخلاصة: تشمل أجهزة التبريد المبردة بناءً على دورة ستيرلنغ ثلاجات أنبوب النبض. غالبًا ما يتم استخدامها في مجموعة متنوعة من التطبيقات ، بما في ذلك استكشاف الفضاء ، والموصلية الفائقة ، والبحث المبرد ، حيث يكون التبريد المبرد الصغير والموثوق به ضروريًا. يتم ضغط الغاز العاملة ، وعادة ما يتم ضغطه وتوسيعه في دورات داخل نظام مغلق لتشغيل ثلاجة أنبوب النبض. الهدف من البحث النظري حول ثلاجات أنبوب النبض هو فهم السلوك الديناميكي الحراري وخصائص الأداء للنظام. من أجل الحصول على أكبر كفاءة تبريد ودرجات حرارة أقل ، تسعى هذه الدراسات إلى تحسين معلمات التصميم وظروف التشغيل. للتنبؤ بأداء النظام ، تأخذ النماذج النظرية في الاعتبار عددًا من المتغيرات ، بما في ذلك نقل الحرارة ، وإسقاط الضغط ، وديناميات الغاز ، وخصائص السوائل. توضح النتيجة كيف تدرج درجة حرارة النظام. تم استخدام برنامج ANSYS لإجراء محاكاة حرارية ، بالإضافة إلى استخدام SoldWorks لرسم تصميم الهندسة ، يكون التدرج درجة الحرارة هو 3 واط/م 2 ، حيث يصل الحمل الحراري إلى ارتفاع درجة الحرارة مع ارتفاع درجة الحرارة ، حيث يصل [43،58،79 ، 90،111،156] k في [3،4،5،6،8،10] w/m2. مع تدرج درجة الحرارة 103.119 K في الترتيب الأول و 113.360 K بالمنتدى الثاني ، يوضح نهج المحاكاة أن أفضل السيناريو حقق 105 K. أفضل مثال مع اختلاف في الحمل الحراري في 3 W/M2 ، حيث وصل إلى K108 ، كشفت النتائج عن انخفاض درجة حرارة معدل الخطأ بنسبة 5 ٪ في أنبوب النبض.

1. Introduction

The cryogenics is the study of phenomena that occurs at extremely low temperatures, often referring to cryocoolers. These devices are typically small, tabletop-sized systems with input powers under 20 kW, or even larger ones used to cool superconducting magnets in molecule gas pedals. The cryogenic liquid is typically burned through a

thermodynamic cycle by moving parts, typically at normal temperature, precooled in an intensity exchanger, and then passed. The pulse tube cooler (PTR), also known as a PTR, is an advanced device that can be built without moving components in the low-temperature area, making it suitable for various applications. The development of cryogenic temperatures has expanded due to the need for more efficient cooling systems [1]. The PTR is currently the best cryocooler for a given size and is used in space missions to cool infrared central plane displays. Researchers develop and refine models based on thermodynamics, fluid mechanics, and heat transfer principles to better understand the system behavior and optimize its performance[2]. By studying the thermal performance of pulse tube refrigerators, researchers aim to improve their efficiency, cooling power, and temperature range. This knowledge contributes to the development of advanced cryogenic technologies and enables their application in various fields, such as medicine, space exploration, and scientific research[3,4 ,10,11].

Fig.1: Three-layered

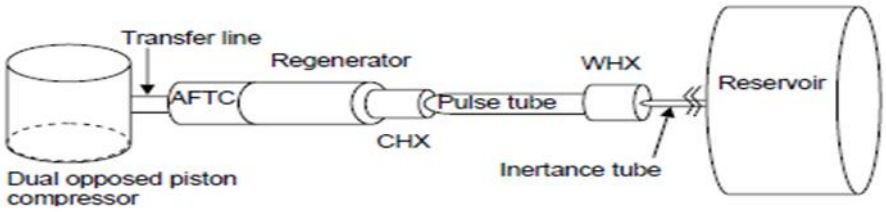

perspective on the inertance beat tube fridge [8].

2. Methodology

A valveless compressor acts directly to produce the pressure waves within a Stirling-type pulse tube refrigerator. Consequently, Stirling-type pulse tube refrigerators operate most often at high frequencies . Except the compressor, which is substituted by a dual opposed piston model in the current simulation, the dimensions of the Stirling type inertance tube pulse tube refrigerator (ITPTR) is derived from literature [5]. The inertance tube pulse tube refrigerator systems of relevance in the current simulations are shown in three dimensions in Figure 3. demonstrates that the ITPTR system's individual parts are all cylindrical in shape and are arranged in a series to produce an axis-symmetric system. In order to simulate the ITPTC, an axis-symmetric, two-dimensional coordinate system was used[13]. The shape of ITPTR produced using solidworks program is shown in Figure 2. The system is first physically depicted utilizing solidworks software in a two-dimensional, axis-symmetric coordinate system. The whole geometry produced as a single component, then it is divided into several zones. The purpose of splitting is to separate the geometry into distinct components so that, when required, alternative boundary conditions may be applied at various zones. The entire meshing of the various ITPTR components' axis-symmetric shape is shown in further detail in Figure 3.3.The model boundaries must be established once the model has been generated and exported to Fluent [5] as shown Table 1.

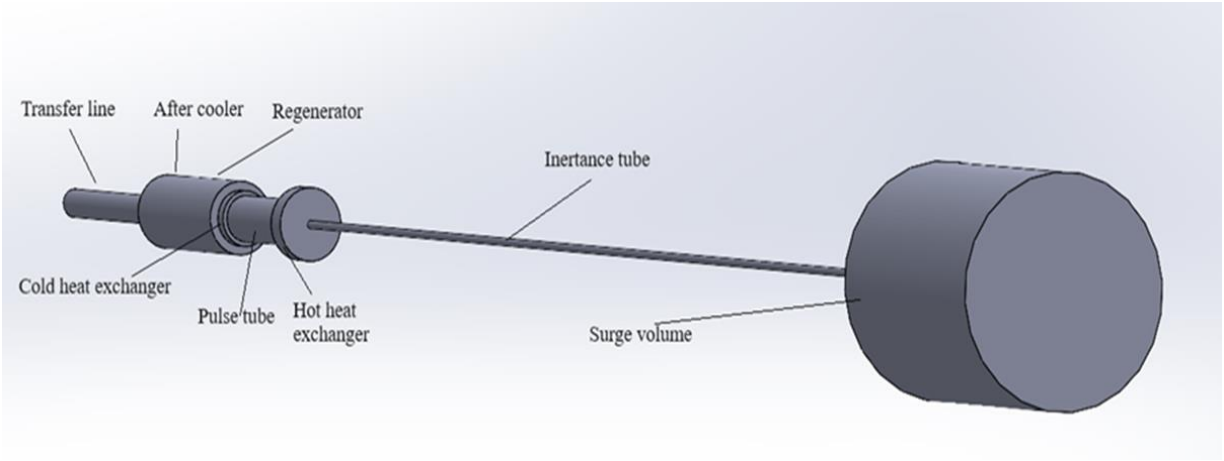

Fig.2: Geometry design.

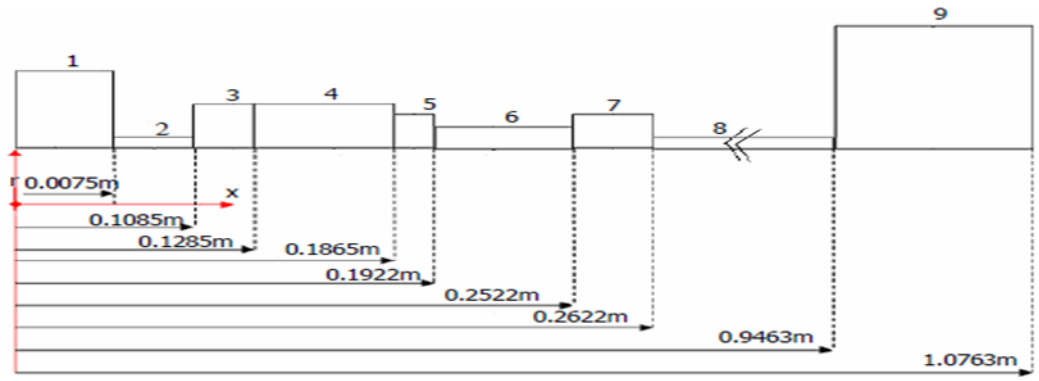

Fig.3: 1-compressor,2-move line,3-after cooler 4-regenerator,5-cold intensity exchanger,6-beat tube,7-hot intensity exchanger,7-inertance tube ,9-flood volume

Two-layered pivot symmetric math of ITPTR [8].

Table (1): Component dimensions of ITPTR

SNo.	Components	Radius (m)	Length (m)
1	Compressor	9.54E − 03	7.50E − 03
2	Transfer line	1.55E − 03	1.01E − 01
3	After cooler	4.00E − 03	2.00E − 02
4	Regenerator	4.00E − 03	5.8E − 02
5	Cold heat exchanger	3.00E − 03	5.7E − 03
6	Pulse tube	2.5E − 03	6.0E − 02
7	Hot heat exchanger	4.00E − 03	1.0E − 02
8	Inertance tube	4.25E − 04	6.84E − 01
9	Surge volume	1.30E − 02	1.3E − 01

.

3. Mesh generation

Generally, unstructured matrices are effective for complex calculations, so for the above reason, the unstructured tetrahedron frameworks was utilized in the ongoing review. ANSYS supports solid geometry mesh generation and three-dimensional models with minimum input from a single phase from the user. The number of cells taken in this study was (1755236) tetrahedron element, and sizing of element 15mm, as shown figure 4. The same mesh configuration formula was used for all cases so that there would be no difference in the results.

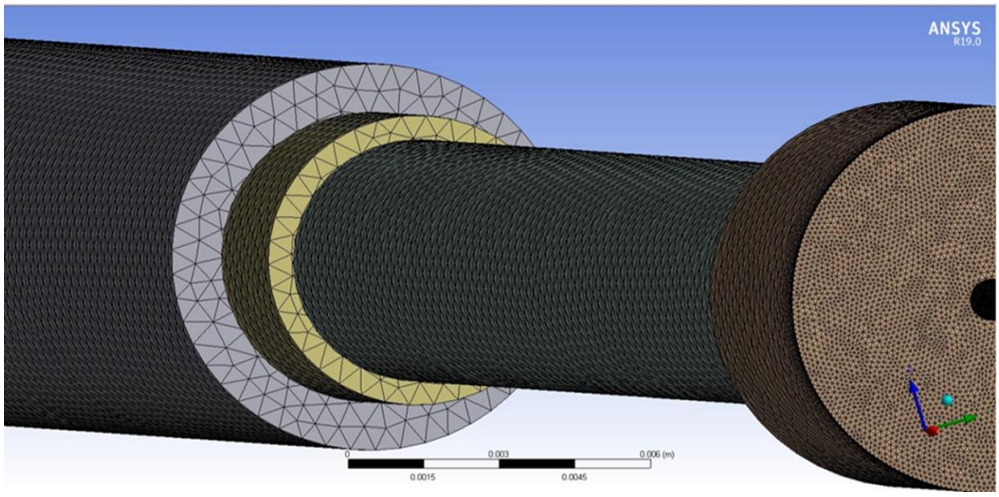

Fig 4: Mesh generated

3.1 Improvement of CFD accuracy

Checking the mech accuracy, precision, and stability of numerical computations is greatly influenced by the mesh quality. Regardless of the mesh type used in the domain, checking the mesh quality is critical. A generated mesh's quality can be controlled and defined in a variety of ways. The thesis delves deeper checking test the methods which were element skewness as shown in Table 2.

• Skewness: It is described as the difference in shape between the cell, and an equilateral cell of equivalent volume. If the average skewness is greater than 0.33 then upgrading of mesh should be considered.

Case	Skewness		
	Min.	Max.	Avg.
416366	1.6028×10^{-4}	0.91839	0.23472

3.2 Mesh Independency

The simulation process requires the work of complex algorithms to solve the matrices contained in the domain, and therefore an accurate network must be made to solve the equations. And then work on the reliability of the

mesh for a solution to reach a stable state with the results. Because of the multiplicity of models that have been simulated, it is necessary to make more than one network and more than one mesh reliability. The number of the elements was 2399443 when the minimum temperature in the pulse tube reached 87.12 K as shown in Table 3.

Table (3): Mesh independency test

Case	No .of Elements	No. 0f Nodes	Minimum temperature in pulse tube (K)
1	416366	110648	102.8
2	644679	163271	93.53
3	1124718	268030	88.03
4	2399433	530645	87.12

4. Governing equations

The condition for the state of movement is as per the following [16 ,17,18]:

$$\frac{\partial p}{\partial t} + \nabla.(\rho v) = s\,m \qquad \ldots\ldots\ldots\ldots\ldots \quad (1)$$

In condition one it is because of general development, but in condition 2 the condition is as a course, or if nothing else, it is in a remarkable case, as it is given in the going with structure

$$\frac{\partial p}{\partial t} + \frac{\partial(\rho v_x)}{\partial x} + \frac{\partial(\rho v r)}{\partial r} + \frac{(\rho v r)}{r} = sm \qquad \ldots\ldots\ldots\ldots\ldots \quad (2)$$

where x is the crucial heading, r is the winding bearing, v_x is the center speed, and v_r is the excessively long speed [18].

Assurance of power in an inertial (non-accelerating)

$$\frac{\partial(\rho V^{\rightarrow})}{\partial t} + \nabla.(\rho v^{\rightarrow} v^{\rightarrow}) = -\nabla p + \nabla.(\tau^{-})^{-} + \rho g^{\rightarrow} + F^{\rightarrow} \quad \ldots\ldots\ldots \quad (3)$$

where p is the static strain, τ^{-} is the strain tensor (portrayed under), and ρg $^{\rightarrow}$ and F $^{\rightarrow}$ are the gravitational body power and outside body powers (for example, that rise out of relationship with the dispersed stage), independently. F $^{\rightarrow}$ in this manner contains other model-subordinate source terms, for instance, penetrable media and client portrayed sources [9]. The strain tensor τ^{-} is given by

$$(\tau^{-})^{-} = \mu\left[\nabla V^{\rightarrow} + \nabla V^{\rightarrow T}\right] - \frac{2}{3}\nabla.V^{\rightarrow} I] \qquad \ldots\ldots\ldots\ldots\ldots \quad (4)$$

where μ is the nuclear consistency, I is the unit tensor, and the second term on the right hand side is the effect of volume expansion [18].

For 2D axisymmetric calculations, the middle point and expanded power confirmation conditions are given by

$$\frac{\partial(\rho V\,X)}{\partial t} + \frac{1}{r}\frac{\partial}{\partial x}(r\rho v_x v_r) + \frac{1}{r}\frac{\partial}{\partial r}(r\rho v_r\, v_x) = -\frac{\partial p}{\partial x} + \frac{1}{r}\frac{\partial}{\partial x}\left[r\mu\left(2\left(\frac{\partial(vx)}{\partial x} - \frac{2}{3}(\nabla.v^{\rightarrow})\right)\right] + \frac{1}{r}\frac{\partial}{\partial r}(r\mu(\left(\frac{\partial v}{\partial r}x\right) + \left(\frac{\partial v}{\partial x}r\right) + F_x \ldots \quad (5)$$

And

$$\frac{\partial}{\partial t}(\rho vr) + \frac{1}{r}\frac{\partial}{\partial x}(r\rho v_r v_x) + \frac{1}{r}\frac{\partial}{\partial r}(r\rho v_r v_x) = -\frac{\partial p}{\partial r} + \frac{1}{r}\frac{\partial}{\partial x}\left(r\mu\left(\frac{\partial v_r}{\partial x}\right) + \frac{\partial v_x}{\partial r}\right) + \frac{1}{r}\frac{\partial}{\partial r}(r\mu\left(2\frac{\partial v_r}{\partial r}\right) - \frac{2}{3}(\nabla . v^{\rightarrow}))) - 2\mu_{(r^r)} + \frac{2}{3}\frac{\mu}{r}(\nabla . v^{\rightarrow})\frac{\rho v_r}{r} + F_r + \ldots \quad (6)$$

where

$$\nabla . v^{\rightarrow} = \left(\frac{\partial}{\partial x}vx\right) + \left(\frac{\partial}{\partial r}vr\right) + \frac{v_r}{r} \ldots\ldots\ldots\ldots \quad (7)$$

what's more v_r is the spin speed [18].

4. Results and discussion

4.1 Validation with Yamuna Of IPTR

A comparison was made with previous research [8]. to ensure the validity of the work presented. And adherence to the steps that have been taken in terms of forming a stereoscopic with dimensions similar to the previous research and the same boundaries used, where results were obtained for the temperature drop at the pulse tube, compared with an error rate that does not exceed 5%, as in Figure 6.

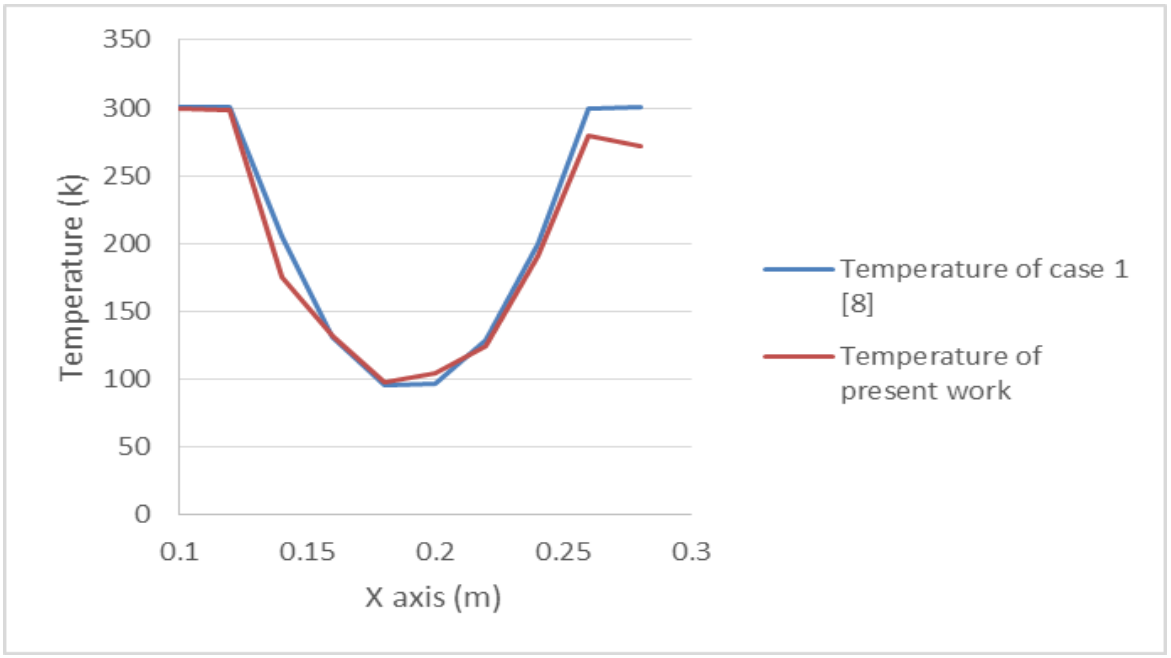

Fig.6: Temperature validation of IPTR .

4.2 Inertance tube pulse tube refrigerator (IPTR)

The Inertance Tube Pulse Tube Refrigerator (IPTR) is an advanced cooling system that uses thermodynamic principles to achieve cryogenic temperatures. It is a family of pulse tube refrigeration systems with a compressor, pulse tube, inertance tube, and regenerator. The compressor compresses working gas to high pressure, while the inertance tube separates compression and expansion phases, improving efficiency. The pulse tube is connected to a regenerator, which transfers heat between the working gas and the cold side, enhancing cooling performance. The inertance tube controls gas dynamics and enhances cooling performance[14]. The ITPTR's advantages include its compact design, excellent cooling performance, and its ability to operate without moving parts in the cold section. It is used in various fields, including scientific research, aerospace, and medical industries, for cooling superconducting devices, cryopumps, detectors, and other equipment requiring extremely low temperatures.

4.2.1 Case 1: known heat load boundary condition

In Figure (7), which shows the temperature gradient with the difference in deferent heat load, when it is noted that the best case reached is at 3 W / m ^{2}, due to it reaching a temperature of 47 K, which is the best case from the remaining cases.

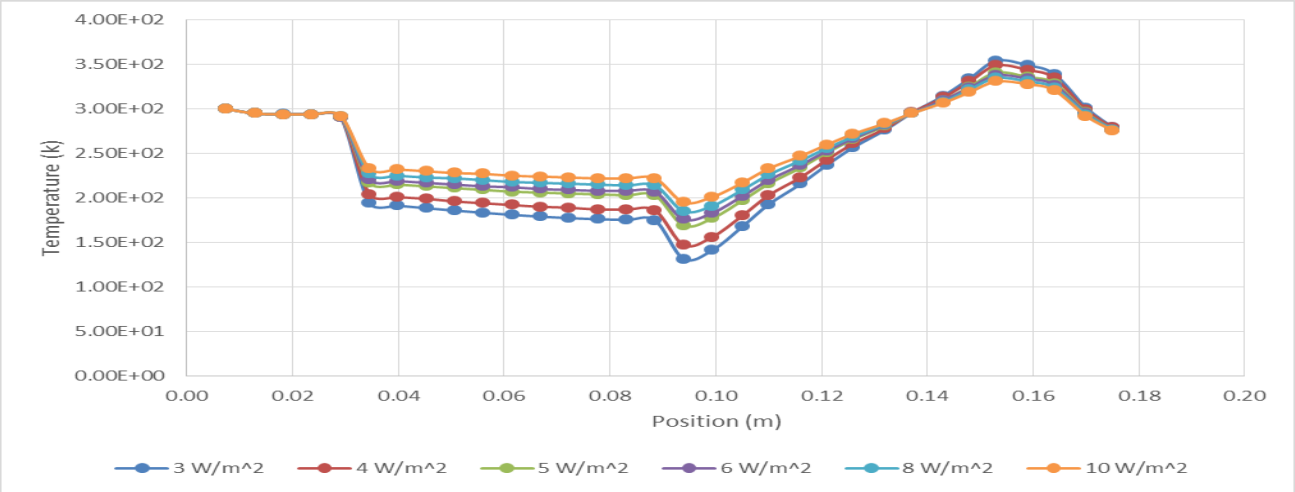

Figure 7: Temperature gradient with differences heat load

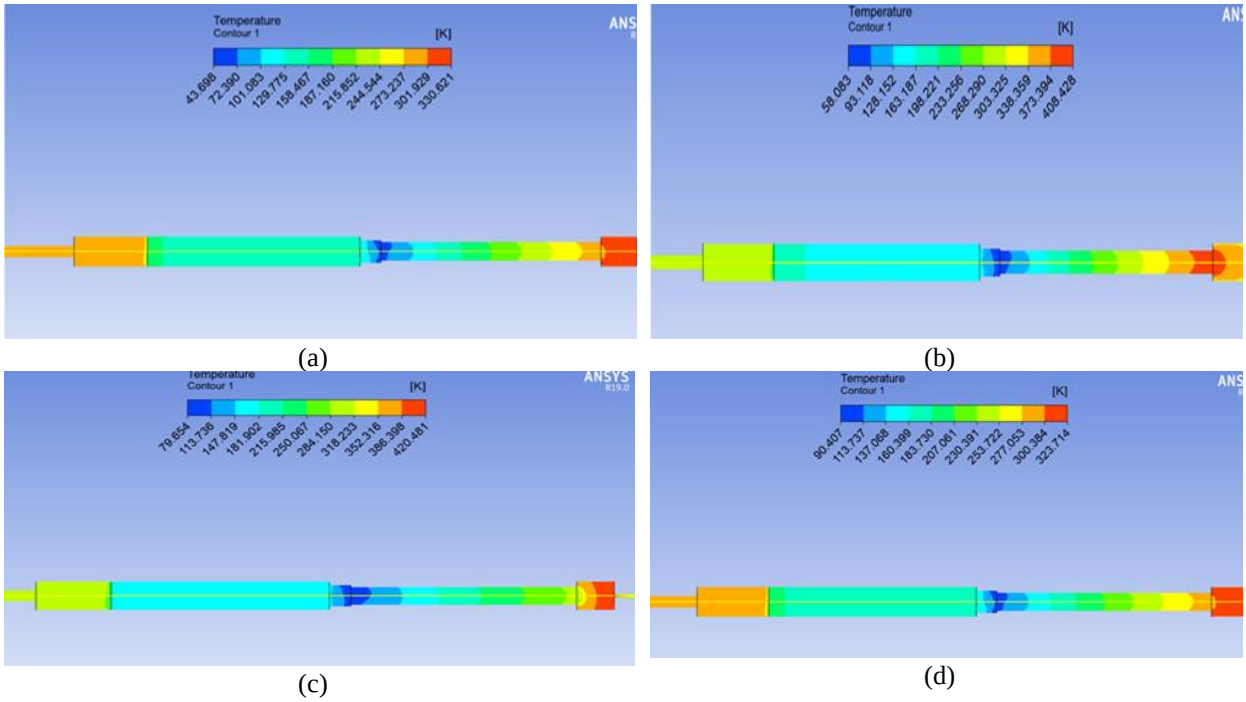

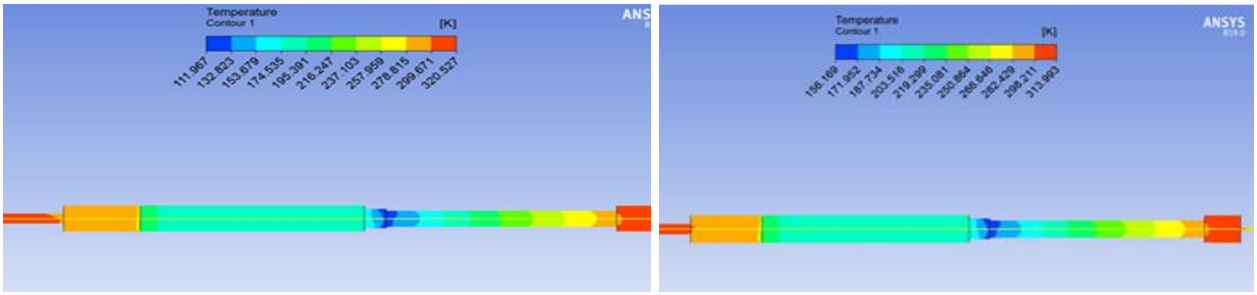

(e) (f)

Figure 8: Temperature contour at. (a) 3 W/m2 heat load,(b) 4 W/m^2 heat load, (c) 5 W/m^2 heat load, (d) 6 W/m^2 heat load, (e) 8 W/m^2 heat load, (f) 10 W/m^2 heat load

Fig.7 shows that the temperature value has decreased with the decrease in the heat flux value .I t is noticed that the case 3 W/m^2 heat load arrived at a temperature of 43 k, while in the event that 4 W/m^2 heat load the temperature arrived at 58 k while on the off chance that 5 W/m^2 heat load, the temperature arrived at 79 k, while on account of 6 W/m^2 heat load, the temperature arrived at 90 k, while on account of 8 W/m^2 heat load, the temperature arrived at 111 k On account of 10 W/m^2 heat load, the temperature arrived at 156 k

4.2.2 Case 2: isothermal boundary condition

In Figure (9), which shows the temperature gradient with deferent isothermal boundary condition. When it is noticed that the best condition reached is at 100k, and that is because it reached a temperature of 79k, the best condition from the remaining cases.

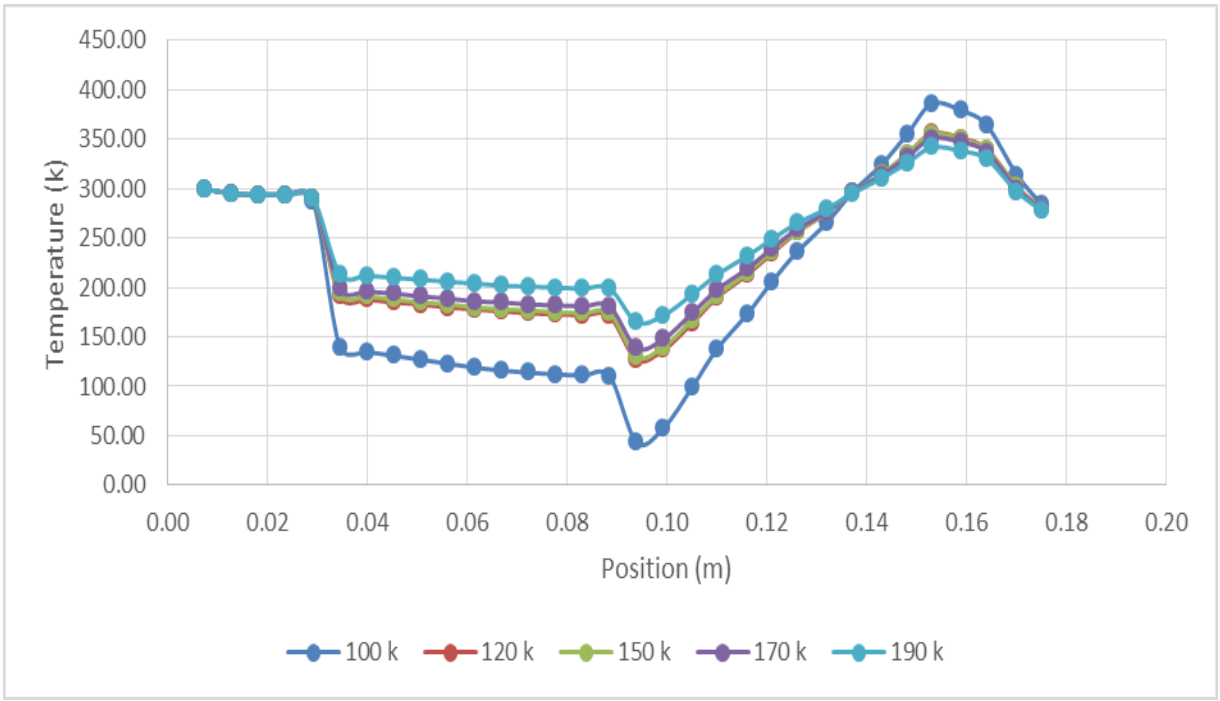

Figure 9: Temperature gradient with different isothermal boundary condition.

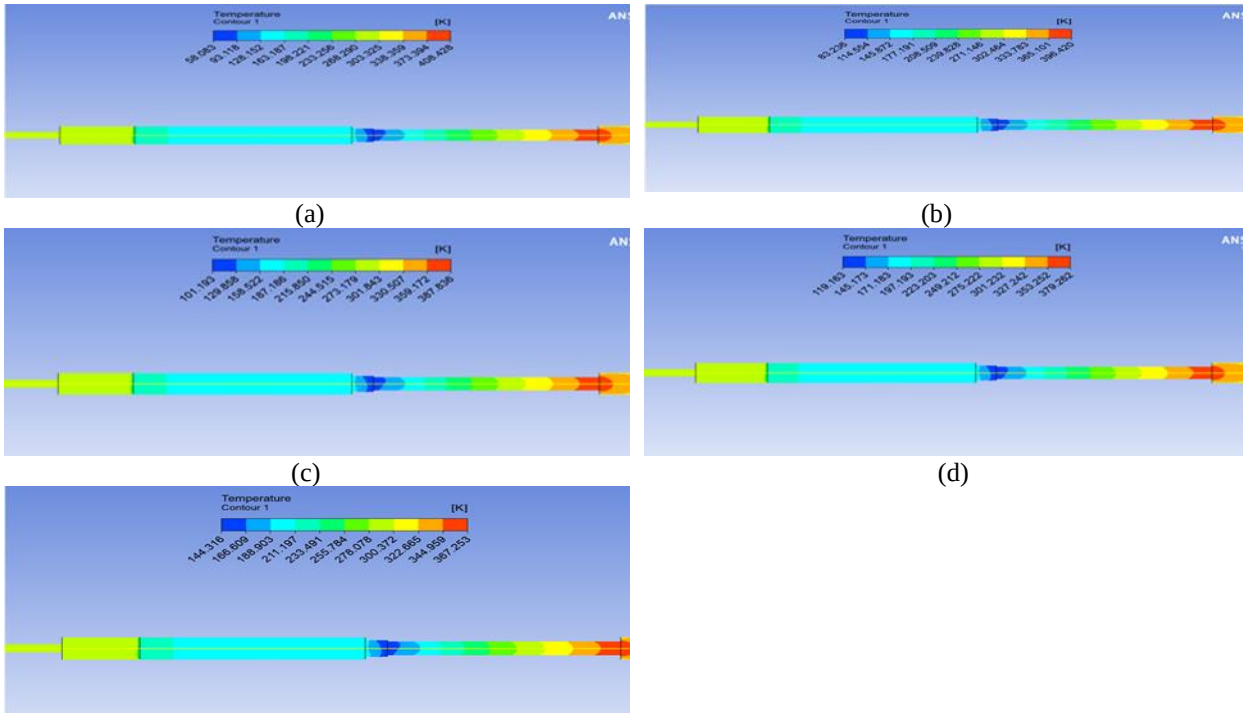

Figure 10: Temperature contour at. (a) 100 k isothermal boundary condition, (b) 120 k isothermal boundary condition, (c) 150 k isothermal boundary condition, (d) 170 k isothermal boundary condition, (e) 190 k isothermal boundary condition.2

In Figure (10) it is noted that case 100k isothermal boundary condition the temperature reached 58 k, while in case 120k isothermal boundary condition the temperature reached 83 and in case 150k isothermal boundary condition the temperature reached The temperature reached 101 k, while in the case 170k isothermal boundary condition, the temperature reached 119 k , while in the case of 190kisothermal boundary condition, the temperature reached 144 k.

4.3 Orifice pulse tube refrigerator (OPTR)

4.3.1 Case 1: known heat load boundary condition

In Figure (11), which shows the temperature gradients with the difference in heat load, when it is noted that the best case reached is at 3 W / m ^ 2, and that is because it reached a temperature of 131 k, the best case of the remaining cases.

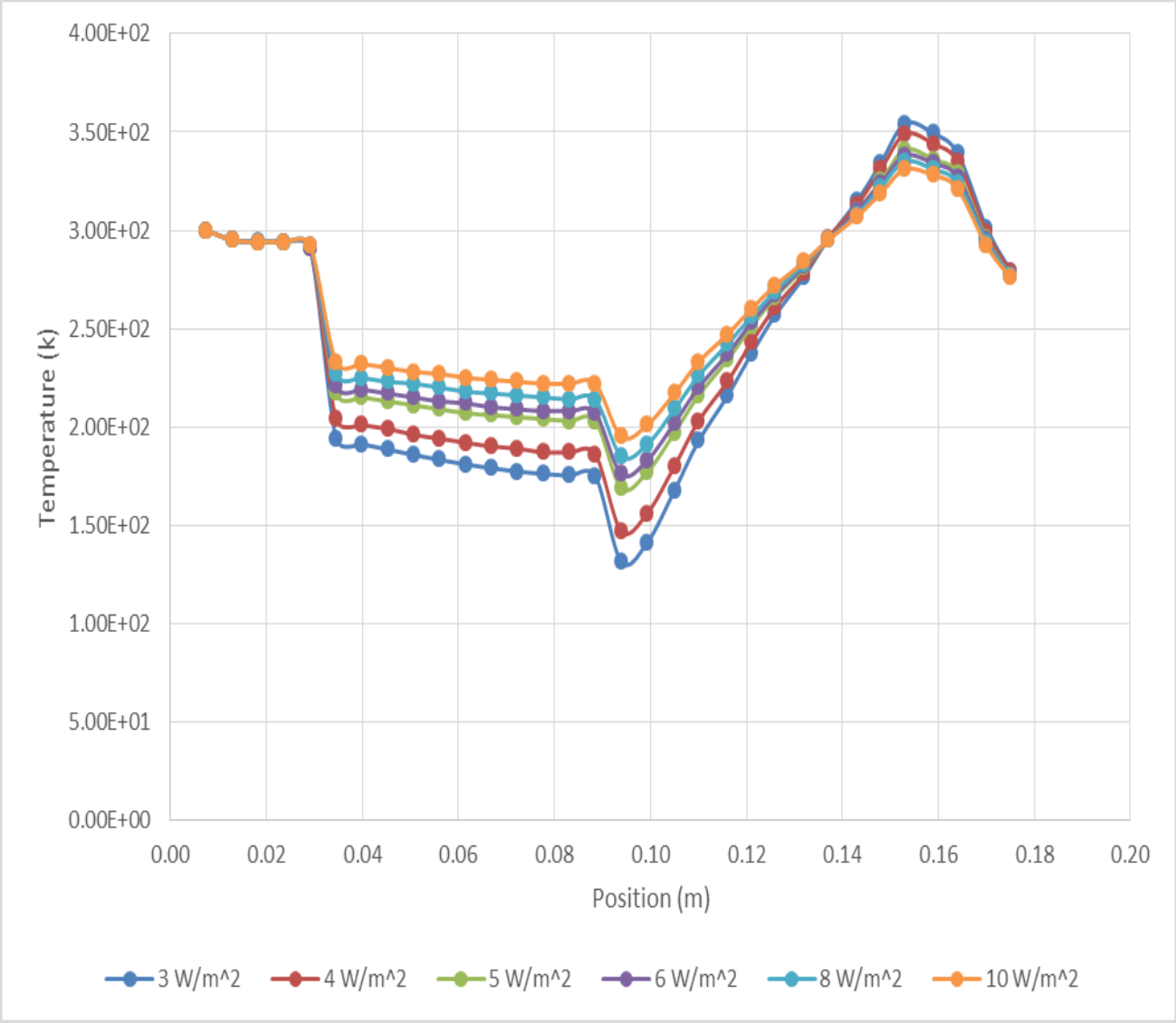

Figure 11: Temperature gradient with deferent heat load

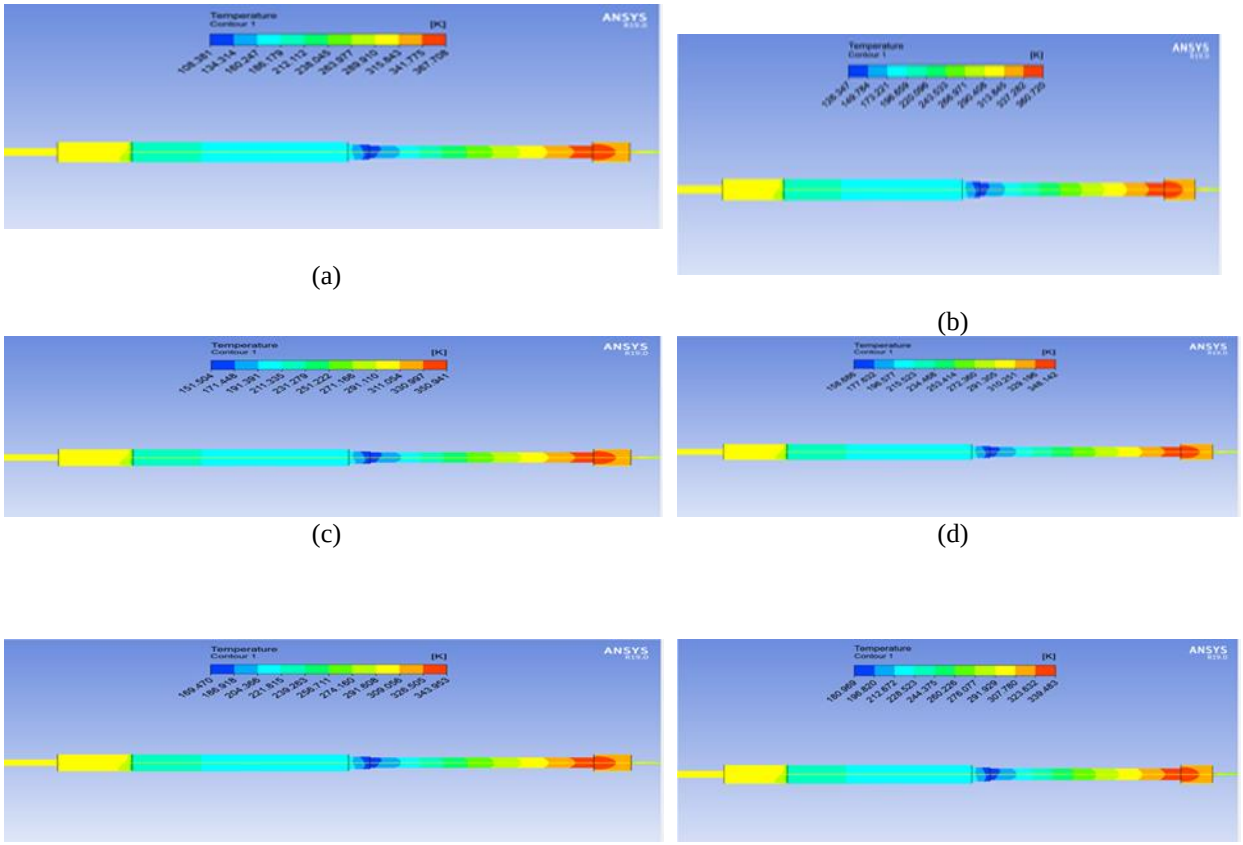

Figure 12: Temperature contour at. (a) 3 W/m^2 heat load, (b) 4 W/m^2 heat load, (c) 5 W/m^^{2} heat load, (d) 6 W/m^2 heat load, (e) 8 W/m^2 heat load, (f) 10 W/m^2 heat load

In Figure (12) it is noticed that the case 3 W/m^2 heat load arrived at a temperature of 108 k, while on the off chance that 4 W/m^2 heat load the temperature arrived at 126 k while in the event that 5 W/m^2 heat load, the temperature arrived at 151 k, while on account of 6 W/m^2 heat load, the temperature arrived at 158 k, while on account of 8 W/m^2 heat load, the temperature arrived at 169 k On account of 10 W/m^2 heat load, the temperature arrived at 180 k.

4.3.2Case 2: isothermal boundary condition

In Figure (13), which shows the temperature gradient with deferent isothermal boundary condition. When it is noticed that the best condition reached is at 100k, and that is because it reached a temperature of 48k, the best condition from the remaining cases.

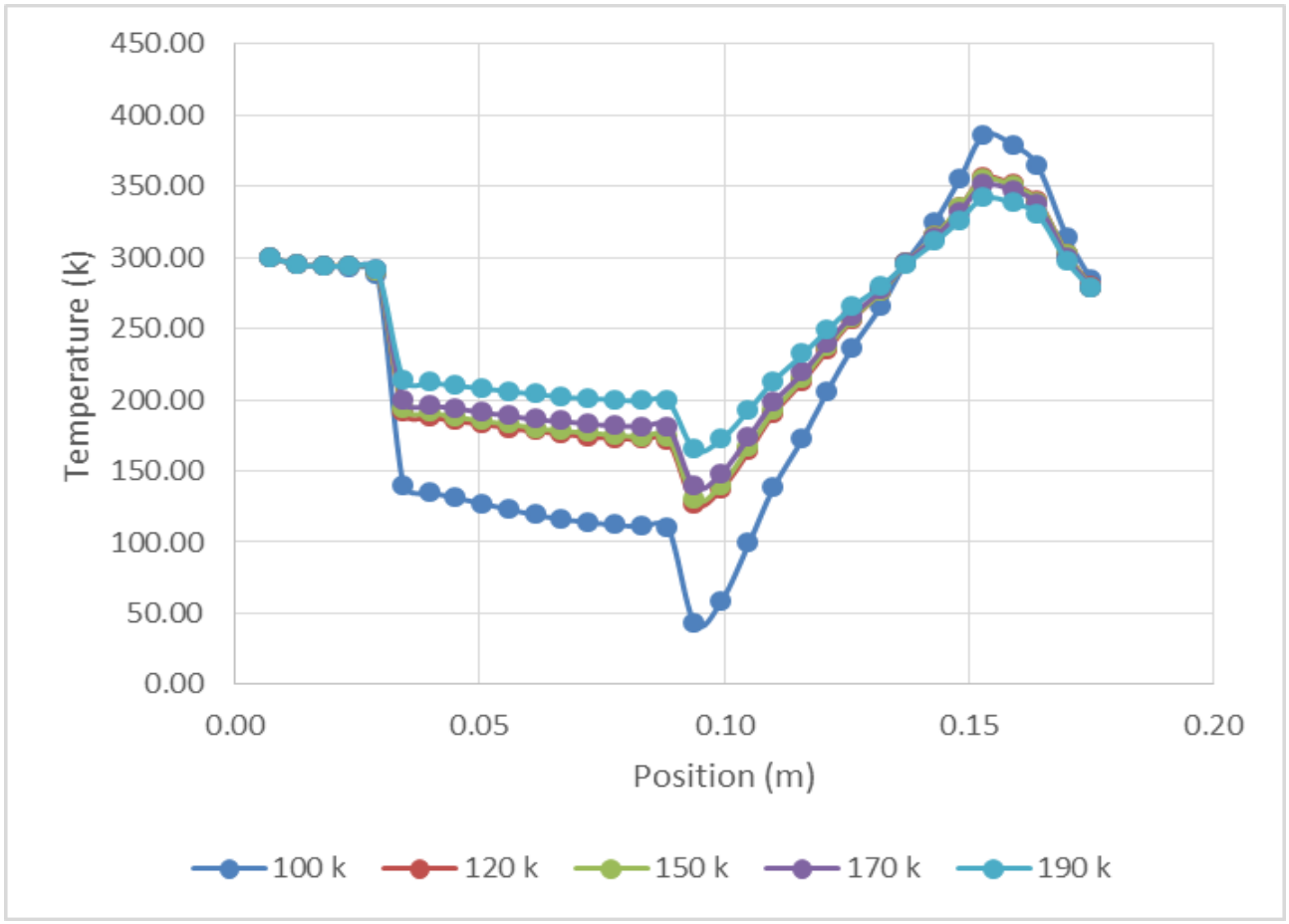

Figure 13: Temperature gradient with deferent isothermal boundary condition.

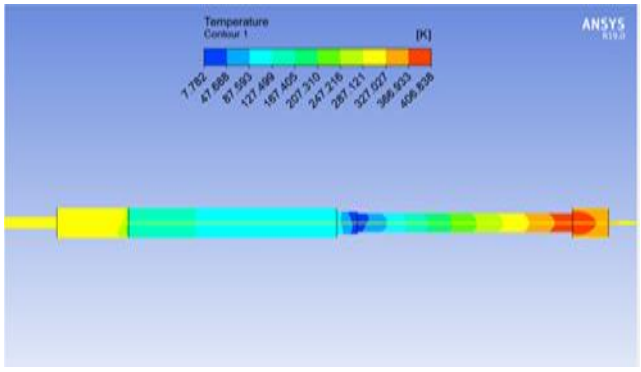

(a)

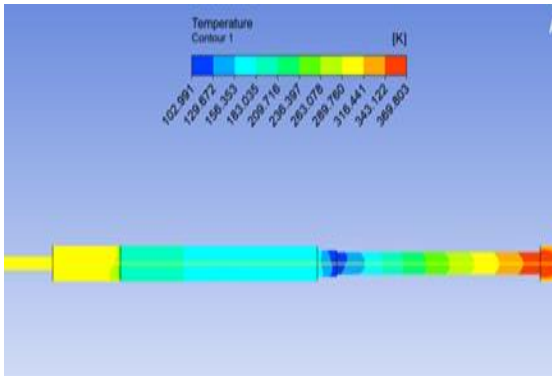

(b)

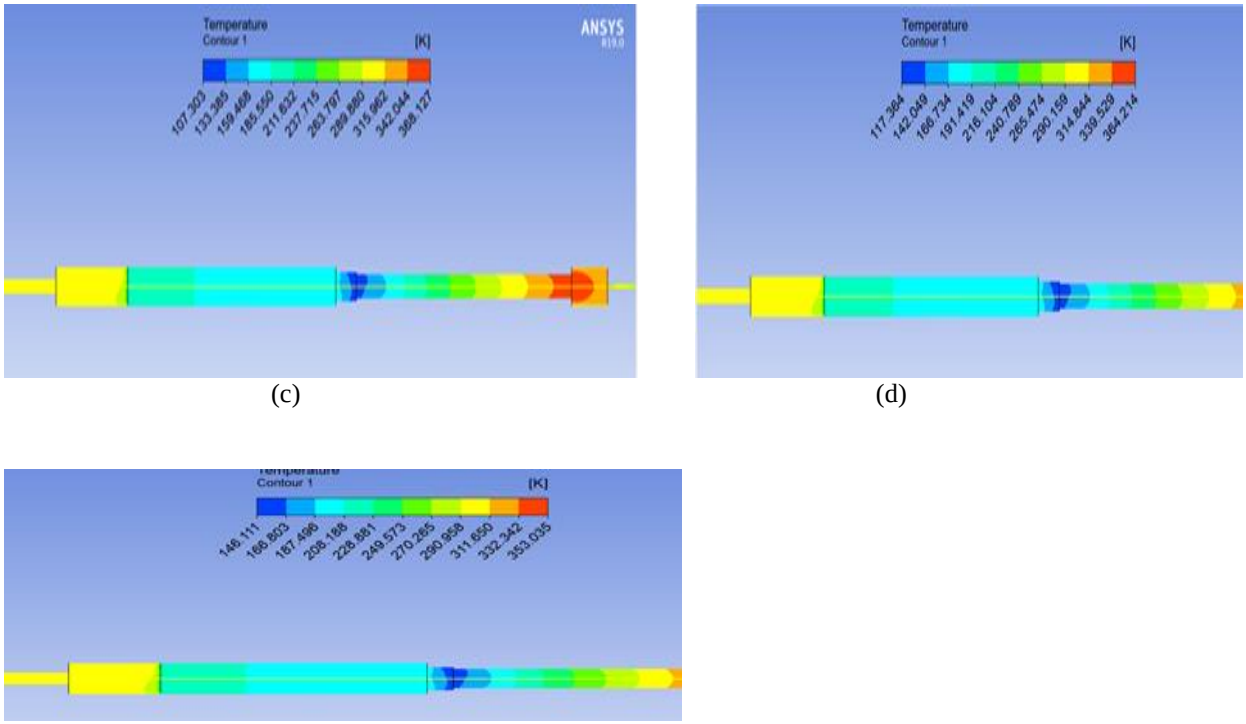

(c) (d)

(e)

Figure 14: Temperature contour at. (a) 100 k isothermal boundary condition, (b) 120 k isothermal boundary condition, (c) 150 k isothermal boundary condition, (d) 170 k isothermal boundary condition, (e) 190 k isothermal boundary condition.

In Figure (14) it is noted that case 100k isothermal boundary condition the temperature reached 47 k, while in case 120k isothermal boundary condition the temperature reached 102 k and in case 150k isothermal boundary condition the temperature reached The temperature reached 107 k, while in the case 170k isothermal boundary condition, the temperature reached 117 k , while in the case of 190kisothermal boundary condition, the temperature reached 146 k.

5 **Conclusion**

1- The temperature gradient in a system is observed with longitudinal distance, with the first order having a lower temperature rise and the second order reaching 340 K at the hot heat exchanger. The lowest temperature is 88.034 K, while the best case is the second order.
2- The temperature gradient varies depending on the deferent heat load, with the best case being 3 W/m^2, which reached 47 K. Other cases include 4 W/m^2, 58 K, 79 K, 90 K, 111 K, and 156 K. The best condition with deferent isothermal boundary conditions is 100k, with a temperature of 79 K. The isothermal boundary conditions vary, with varying temperatures for different isothermal conditions.
3- The temperature gradients vary depending on the heat load, with the best case reaching 131 k at 3 W/m^2. The best condition with different isothermal boundary conditions is at 100k, with temperatures reaching 47 k at 100k, 102 k at 120k, 150 k at 107k, 170k at 117k, and 146 k at 190k. The best condition from the remaining cases is 100k, which reached 48k at 100k.

REFERENCES

[1] Gifford, W.E. and Longsworth, R.C. Pulse tube refrigeration, Trans ASME B J Eng Industry 86(1964), pp.264-267.

[2] Gardner D.L., Swift G.W., Use of inertance in orifice pulse tube refrigerators, Cryogenics, 37(1997), pp. 117-121.

[3] Meddeb, Zina, et al. "Thermodynamic Study of the Active Magnetic Regenerative Refrigeration in Transitional Regime." International Journal of Fluid Mechanics & Thermal Sciences, vol. 1, no. 3, 2015, pp. 49–53, https://doi.org/10.11648/j.ijfmts.20150103.12. Accessed 11 Aug. 2023.

[4] de Boer, P. C. T., Performance of the inertance pulse tube , Cryogenics 42(2002),pp. 209-221.

[5] Rawat, Vivek. Theoretical and Experimental Studies on Pulse Tube Refrigerator. 2015.

[6] Wei Dai, Jianying Hu and Ercang Luo, Comparison of two different ways of using inertance tube in a pulse tube cooler, Cryogenics 46(2006), Pages 273-277.

[7] Cha, J.S. Ghiaasiaan S.M, Desai P.V. Harvey J.P and Kirkconnell C.S. "Multidimensional flow effects in pulse tube refrigerators" Cryogenics 46 (2006) 658–665.

[8] Banjare, Y.P., et al. "CFD Simulation and Experimental Validation of a GM Type Double Inlet Pulse Tube Refrigerator." Cryogenics, vol. 50, no. 4, Apr. 2010, pp. 271–280, https://doi.org/10.1016/j.cryogenics.2010.01.013

[9] Ju Y. L., Wang C. and Zhou Y. ,Numerical simulation and experimental verification of the oscillating flow in pulse tube refrigerator, Cryogenics, 38(1998), pp.169-176.

[10] Wang, C., Wu, P. and Chen, Z., Numerical analysis of double-inlet pulse tube refrigerator, Cryogenics33 (1993), pp.526-530.

[11] Harold Mirels Double inlet pulse tube cryocooler with steeped piston compressor, Advances in cryogenic engineering 39(1994), pp.1425-1431.

[12] Zhu Shaowei, Kawano Shin, Nogawa Masahumi and Inoue Tatsuo, Work loss in double-inlet pulse tube refrigerators .Cryogenics, 38(1998) ,pp. 803-807.

[13] Kirkconnell, C. S. 1995. Numerical analysis of the mass flow and thermal behavior in high-frequency pulse tubes. Ph.D. Thesis, Georgia Institute of Technology, Atlanta, Ga.

[14] Zhu Shaowei and Chen Zhongqi, Enthalpy flow rate of a pulse tube in pulse tube refrigerator. Cryogenics, 38(1998), pp.1213-1216.

[15] Thummes G. and Heiden C. Control of DC gas flow in a single-stage double-inlet pulse tube cooler Cryogenics 38 (1998) 843–847C. Institute of Applied Physics, University of Giessen,

[16] Liang, J., Ravex, A. and Rolland, P., Study on pulse tube refrigeration Part 1: Thermodynamic nonsymmetry effect .Cryogenics, 36(1996), pp. 87-93.

[17] Zhu Shaowei, Wu Peiyi and Chen Zhongqi, Double inlet pulse tube refrigerators: an important improvement, Cryogenics30 (1990), pp. 514-520.

[18] "Ansys | Engineering Simulation Software." Www.ansys.com, ansys.com.